Electronic Signatures of Large Amplitude Motions: Dipole Moments of Vibrationally Excited Local-Bend and Local-Stretch States of S_0 Acetylene†

Bryan M. Wong, Adam H. Steeves, and Robert W. Field*

Department of Chemistry, Massachusetts Institute of Technology, Cambridge, Massachusetts 02139

Received: March 28, 2006; In Final Form: July 19, 2006

A one-dimensional local bend model is used to describe the variation of electronic properties of acetylene in vibrational levels that embody large amplitude local motions on the S_0 potential energy surface. Calculations performed at the CCSD(T) and MR-AQCC levels of theory predict an approximately linear dependence of the dipole moment on the number of quanta in either the local bending or local stretching excitation. In the local mode limit, one quantum of stretching excitation in one CH bond leads to an increase of 0.025 D in the dipole moment, and one quantum of bending vibration in the CCH angle leads to an increase of 0.068 D. The use of a one-dimensional model for the local bend is justified by comparison to the well-established polyad model which reveals a decoupling of the large amplitude bending from other degrees of freedom in the range of $N_{\mathrm{bend}} = 14-22$. We find that the same one-dimensional large amplitude bending motion emerges from two profoundly different representations, a one-dimensional cut through an ab initio, seven-dimensional Hamiltonian and the three-dimensional ($\ell = 0$) pure-bending experimentally parametrized spectroscopic Hamiltonian.

I. Introduction

Even on well-isolated electronic potential surfaces, a large amplitude nuclear motion can lead to significant distortion of the electronic wave function. This is particularly true in the case of electronic potential energy surfaces in the regions near barriers to chemical rearrangement. Reese et al. have recently demonstrated that electronic Stark spectroscopy may be used to distinguish between conformational isomers on both ground and excited electronic surfaces.[1] For conformational isomers, the changes in dipole moments are primarily due to the relative orientations of functional groups. The electronic wave function is even more severely deformed in the case of chemical isomerization in which chemical bonds are broken and new bonds formed, thereby altering the global electronic structure.

A change in electronic structure associated with a particular class of large amplitude motion may also serve as a spectroscopic signature to aid in the assignment of spectra of highly vibrationally excited molecules. Determination of the electric dipole moment has been proposed as a diagnostic of the "isomerization states" that embody large amplitude bending along the reaction coordinate of the HCN ⇌ HNC isomerization.[2] The exceptionally large amplitude bending states on the HCN/HNC potential are electronically distinct from the vast majority of nearly isoenergetic vibrational eigenstates in that the isomerization states sample both the HCN and HNC configurations, resulting in a partial cancellation of the oppositely signed electric dipole moments. Since the vibrational amplitude on both sides of the HCN ⇌ HNC barrier increases with higher excitation in the bending/isomerization coordinate, the measured magnitude of the dipole can be used as a measure of progress along the reaction coordinate.

Eigenstates embodying large amplitude motion make up an exceedingly small fraction of the total number of vibrational states. The vast majority of vibrational states are highly "dynamically mixed" or "ergodic" in the sense that internal excitation is distributed among all vibrational degrees of freedom[3]. The observable consequence of this type of vibrational dynamics on electronic structure is distinct from that of the large amplitude motion states. Because the vibrational energy is distributed throughout the molecule, rather than being directed along one particular large amplitude coordinate, the average electronic structure does not significantly deviate from that of the equilibrium nuclear configuration. The deviations are statistical rather than causal. More physically, large amplitude states are outliers by reason of dynamic mechanism rather than statistical fluctuation.

Large-amplitude motion on the acetylene S_0 surface is considerably more complicated than in HCN, due to both the increased number of vibrational modes and to the inversion symmetry of the molecule. This symmetry results in normal modes of vibration that are either symmetric (*g*) or antisymmetric (*u*) with respect to inversion through the center of the molecule. Many studies[4−13] have demonstrated that the vibrational eigenstates of acetylene and similar molecules undergo a *normal-to-local* transition in which the normal modes appropriate to describe small deviations from the equilibrium geometry evolve into local modes in which the excitation is isolated in a single C−H bond-stretch or CCH angle-bend. This evolution of vibrational character is of particular interest for acetylene bending vibrations because the local bending vibration bears a strong resemblance to the reaction coordinate for isomerization from acetylene to vinylidene (Figure 1a and b) with one hydrogen migrating a large distance off the C−C bond axis, while the other hydrogen remains relatively stationary.

Despite the large number of studies of the vibrational overtone spectrum of acetylene, very little information is available regarding the effect of an electric field on the vibrational levels

† Part of the special issue "Robert J. Silbey Festschrift".

* Corresponding author phone: 617 253-1489; fax: 617 253-7030; e-mail: rwfield@mit.edu.

10.1021/jp061924x CCC: $33.50 © 2006 American Chemical Society
Published on Web 08/25/2006

of the S_0 state of this molecule. This is perhaps not surprising considering the symmetric nature of the acetylene molecule. Not only does the definite *g*/*u* symmetry of every rovibrational level dictate that there can be no permanent dipole moment in any field-free eigenstate, but the inversion symmetry of the molecule further restricts the action of the dipole operator to matrix elements off-diagonal in the vibrational quantum numbers. That is, there is no electric dipole moment in acetylene that can lead to a pure rotational transition. These diagonal in vibration but not rotation elements of the dipole operator, which are necessarily equal to zero in a molecule with inversion symmetry, are referred to as *permanent vibrational dipole moments*.

Despite the absence of a permanent vibrational dipole moment, Barnes et al. have analyzed electric field-induced perturbations in $\nu_1 + 3\nu_3$ and $\nu_2 + 3\nu_3$ bands of acetylene at fields up to 300 kV/cm.[14,15] In both cases, the primary effect of the electric field is to mix the optically bright vibrational state with a near-degenerate optically dark state that differs from the bright state by the exchange of one quantum of excitation in the symmetric C−H stretching mode (ν_1, *g*) for one quantum of excitation in the antisymmetric C−H stretching mode (ν_3, *u*), or vice versa. The electric dipole moment function of S_0 acetylene has also been studied by breaking the inversion symmetry through isotopic substitution. Muenter and Laurie first observed the pure rotational transitions of acetylene-*d* in the ground vibrational state.[16] Matsumura et al. subsequently measured states excited in the CCH and CCD bending vibrations and determined the variation of the dipole moment with excitation in these modes to be 0.046 and −0.0336 D/quanta, respectively.[17]

The present paper utilizes a one-dimensional reaction path-like Hamiltonian to put our predictions of these dipole moments on a quantitative basis. This reduced form of the full seven-dimensional Hamiltonian is suitable for our calculations of vibrationally averaged dipole moments of both local stretching and local bending modes. Although multidimensional potential energy surfaces and dipole moment functions of acetylene can presently be calculated with excellent accuracy,[18−22] we hope to obtain physical insight from an effective, one-dimensional ab initio calculation. Our approach to this enormous reduction in phase space dimension is based on the observation that the spectroscopic fitting Hamiltonian, $\mathbf{H}^{\mathrm{eff}}$, exhibits extremely stable, one-dimensional, pure local bending motions. Therefore, we make use of an ab initio Hamiltonian parametrized by a single internal coordinate in which the relevant large amplitude motion is assumed to be decoupled from the other degrees of freedom. Numerical comparisons with other models and experimental data allow assessment of the physical relevance of this reduction.

II. Hamiltonian

The theory of the internal coordinate path Hamiltonian and its variational solution has been described by Tew et al.[23] Their parametrization of a large amplitude motion with a single internal coordinate is based on the work of Hougen, Bunker, and Johns who were among the first workers to include large amplitude motion in their semi-rigid bender model.[24] Other workers, such as Szalay, have extended this approach to account for nonrigid effects of large amplitude internal motion in general molecules.[25] The formulation of Tew et al. is closely related to the reaction path Hamiltonian introduced by Miller, Handy, and Adams[26] with the exception that the internal coordinate path need not be exactly parallel to the minimum energy path. When defining a path to parametrize a large amplitude motion, it should be remembered that the minimum energy path is defined as the steepest descent path from a transition state toward reactants or products.[27,28] More rigorously, the minimum energy path can be expressed by the solution of the differential equation

$$\frac{d\boldsymbol{x}}{d\tilde{s}} = -\frac{\nabla V}{|\nabla V|}, \tag{1}$$

where $\boldsymbol{x}$ is a 3*N* component vector of mass-weighted Cartesian coordinates, $\tilde{s}$ is the path length, and *V* is the potential energy of *N* nuclear displacement vectors. When the minimum energy path is located in mass-weighted coordinates as written in eq 1, it is called an intrinsic reaction coordinate.[27,28] Since the minimum energy path by definition follows the gradient vector of the potential energy, the potential energy at any point on the path can be expanded in terms of the normal coordinates Q_k up to second order:

$$\hat{V} = V_0(\tilde{s}) + (1/2)\sum_{k=1}^{3N-7} \omega_k^2(\tilde{s}) Q_k^2 \tag{2}$$

where $\omega_k^2(\tilde{s})$ are the 3*N*-7 eigenvalues of a projected force constant matrix.

To define a minimum energy path, one commences by optimizing a saddle point on the potential energy surface and then follows the negative gradient of the energy in mass-weighted Cartesian coordinates. However, as Tew et al. have stated, this algorithm is not a numerically sound technique. If insufficiently small steps are taken along the reaction path, one may be unable to locate the minimum accurately at the end of the path. Furthermore, near the saddle point, the optimized geometries may be inaccurate since the first step away from this starting point is along a vector defined without reference to any curvature. The internal coordinate path Hamiltonian used in this work removes many of these problems by parametrizing a path with a single internal coordinate such as a bond length or a valence bend angle. This parametrization guarantees a continuous variation with no numerical complexity since the internal coordinate is a geometric variable and is always well-defined at any point on the path. However, since this path is obtained by scanning relaxed points on the potential surface with a user-chosen internal coordinate, we have not necessarily followed the gradient vector of the molecular potential energy. Whereas the minimum energy path potential energy has no term linear in Q_k, the internal coordinate path potential must have a linear term:

$$\hat{V} = V_0(s) + \sum_{k=1}^{3N-7} g_k(s) Q_k + (1/2)\sum_{k=1}^{3N-7} \omega_k^2(s) Q_k^2 \tag{3}$$

where *s* is a conveniently chosen geometric variable such as an angle, a bond length, or a combination of angles and bond lengths used to parametrize the large-amplitude path. For many cases, the true reaction coordinate can be approximated by a single internal coordinate, and the gradient g_k will be small if the internal coordinate is approximately in the same direction as $\tilde{s}$. In other words, neglecting this gradient term is equivalent to ignoring the minor off-diagonal matrix elements of $g_k(s)Q_k$ in the small-amplitude harmonic quantum numbers.

In the present work, we use the internal coordinate path method with an approximate treatment for the other small-amplitude modes. The theory of the internal coordinate path Hamiltonian for an *N*-atom molecule is expressed in terms of a

single large-amplitude coordinate s, its conjugate momentum $\hat{p}_s$ ($= -i\hbar\{\partial/\partial s\}$), and the coordinates $\mathbf{Q} = \{Q_1,Q_2,...,Q_{3N-7}\}$ and momenta $\hat{P} = \{\hat{P}_1,\hat{P}_2,...,\hat{P}_{3N-7}\} = -i\hbar\{\partial/\partial Q_1,\partial/\partial Q_2,..., \partial/\partial Q_{3N-7}\}$ of the orthogonal small-amplitude vibrational modes. The full quantum mechanical kinetic energy operator in these coordinates is given by

$$\hat{T} = (1/2)\sum_{d,e=1}^{4} \mu^{1/4}(\hat{\Pi}_d - \hat{\pi}_d)\mu_{de}\,\mu^{-1/2}(\hat{\Pi}_e - \hat{\pi}_e)\mu^{1/4} + (1/2)\sum_{k=1}^{3N-7} \mu^{1/4}\hat{P}_k\,\mu^{-1/2}\hat{P}_k\,\mu^{1/4} \quad (4)$$

$\hat{\Pi}$ and $\hat{\pi}$ are four-component operators given by

$$\hat{\Pi} = (\hat{J}_x,\hat{J}_y,\hat{J}_z,\hat{p}_s)$$

$$\hat{\pi} = \sum_{k,l=1}^{3N-7} (B_{kl,x}(s),B_{kl,y}(s),B_{kl,z}(s),B_{kl,s}(s))Q_k\hat{P}_l \quad (5)$$

where $\hat{J}_x$, $\hat{J}_y$, and $\hat{J}_z$ are the components of the total angular momentum operator, and $B_{kl,x}$, $B_{kl,y}$, $B_{kl,z}$, and $B_{kl,s}$ are the "Coriolis coupling" matrices[23] that are functions of the large-amplitude coordinate s. The symmetric tensor, μ_{de}, and its determinant, μ, are also functions of the internal coordinate s.

As reported previously,[29] the following approximations allow for the computation to be manageable: (1) the effective inertia tensor depends weakly on $\mathbf{Q}$, and only the terms that depend on s are retained; (2) the Coriolis terms, $\hat{\pi}_\alpha$, are linear in the small-amplitude coordinates, $\mathbf{Q}$, and their contribution to the kinetic energy is neglected; (3) numerically enforcing the Eckart conditions minimizes many of the coupling terms in eq 4. It follows from these approximations that the kinetic energy operator for total angular momentum $J = 0$ can be written in the following form

$$\hat{T} = (1/2)\hat{p}_s\,I_{0ss}^{-1}\,\hat{p}_s + (1/2)\mu^{1/4}(\hat{p}_s\,I_{0ss}^{-1}\,\mu^{-1/2}(\hat{p}_s\,\mu^{1/4})) + (1/2)\sum_{k=1}^{3N-7} \hat{P}_k^{\,2} \quad (6)$$

where I_{0ss}^{-1} and μ are given by

$$I_{0ss}^{-1}(s) = (\sum_{i=1}^{N} \mathbf{a}_i'(s)\cdot\mathbf{a}_i'(s))^{-1} \quad (7)$$

$$\mu(s) = I_{0ss}^{-1}\cdot\det(\mathbf{I}_0^{-1}) \quad (8)$$

and $\mathbf{I}_0$ is the normal 3×3 Cartesian inertia tensor along the path. The vectors $\mathbf{a}_i$ ($= m_i^{1/2}\mathbf{r}_i$) are the mass-weighted Cartesian coordinates of the ith atom at a point on the path s with respect to the Eckart axis system, and $\mathbf{a}'_i = d\mathbf{a}_i/ds$. Finally, the operator $\hat{p}_s$ operates only within the parentheses in eq 6; that is, the next to last term in eq 6 is a scalar term.

III. Ab Initio Calculations

All ab initio electronic structure calculations for the acetylene−vinylidene isomerization were carried out with the Gaussian 03 package.[30] Extensive theoretical studies have been carried out on both the global potential energy surface[20,21] and the one-dimensional minimum energy path[19] in the current literature. One of the most recent theoretical studies on acetylene is the investigation by Zou and Bowman.[20] Their analysis includes several high-level ab initio calculations of the six-dimensional potential (seven-dimensional for linear geometries) performed at the coupled cluster with single and double substitutions with perturbative triples (CCSD(T)) level of theory. In their least-squares fit of the potential energy surface, they obtained eigenfunctions and eigenvalues of the exact Hamiltonian for zero total angular momentum. The most consistent and accurate ab initio energies are from their CCSD(T)/aug-cc-pVTZ calculations which yield a 15407 cm^{-1} energy difference between the acetylene and vinylidene minima.

Since the goal of this work is to obtain an effective one-dimensional cut of a seven-dimensional potential, we do not intend to reproduce Zou and Bowman's ab initio values exactly. Instead we wish to obtain accurate results from computational methods which do not require the evaluation of gradients or Hessians. To this end, the relaxed geometry parameters were analyzed using the CCSD level of theory with Dunning's augmented correlation consistent triple-ζ basis, aug-cc-pVTZ.[31] The geometry optimizations were carried out with extremely tight convergence criteria with root-mean-square forces within 0.00001 atomic units and root-mean-square displacements within 0.00004 atomic units. CCSD(T) single-point energies were subsequently performed with the cc-pVQZ basis set at the CCSD optimized geometries.

For the acetylene−vinylidene isomerization, we are primarily interested in the local-bender limit of the 1,2-hydrogen rearrangement process. The isomerization coordinate near the linear acetylene global minimum corresponds to an HCC bend-like motion and involves a periodic potential. Therefore, the most appropriate choice for the large-amplitude parameter s is the internal HCC bend angle coordinate. While CC−HH diatom−diatom coordinates are much better suited for describing vinylidene and H-atom orbiting states,[20,21] they are more awkward to use at low energies below the vinylidene isomerization barrier.[32−34] For this reason, we obtained our internal coordinate path by constraining the HCC angle at 5° increments while optimizing all other internal coordinates to minimize the total energy. At all intermediate geometries between the $D_{\infty}h$ acetylene global minimum and the C_{2v} vinylidene local minimum, molecular symmetry was constrained within the C_s point group. It should also be remembered that the domain for the valence angle s is $(0, 2\pi)$; that is, $s = 0$ corresponds to one linear structure ($H_aC_bC_cH_d$), and $s = \pi$ corresponds to another ($H_dC_bC_cH_a$). The permutational symmetry of the isomerization path with respect to the interchange of the two H atoms (P_{ad}) was used to generate additional energies, dipole moments, and geometries. Therefore, the fully symmetric internal coordinate path can be constructed with only the information from vinylidene to acetylene by using permutation group operations in a local frame. The symmetric a-axis and antisymmetric b-axis dipole moment components of acetylene at the CCSD(T)/cc-pVQZ levels of theory are shown in Figure 2a. Since all molecular geometries were constrained to lie in a plane, the c-axis dipole moment is exactly zero, and only the a-axis and b-axis dipole components are displayed. Finally, each resulting geometry was translated to the center of mass frame, and all energies, dipole moments, and geometries as a function of s were fit to a Fourier series. In this way, finite differences can be used to solve iteratively for the Euler angles that rotate the Cartesian axes in order to impose the Eckart conditions.

A converged set of eigenvalues and eigenvectors for the one-dimensional Hamiltonian described in eq 6 were computed using a discrete variable representation.[35] For the acetylene−vinylidene isomerization, the large-amplitude coordinate involves a periodic potential, and the most natural choice for a

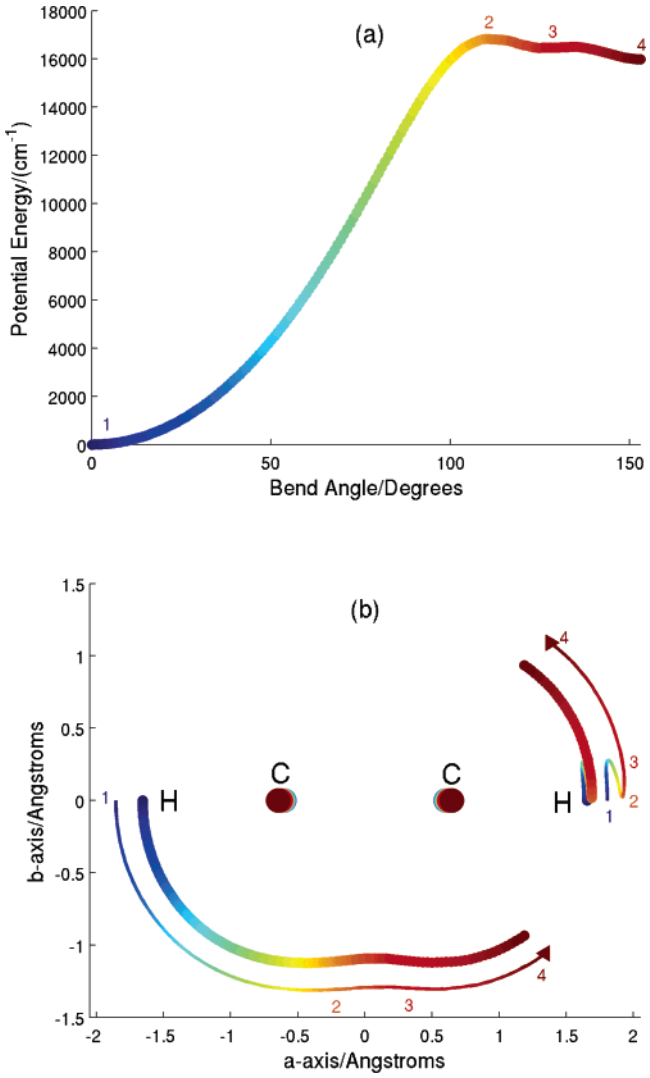

Figure 1. (a) One-dimensional relaxed potential for the acetylene−vinylidene isomerization as a function of the HCC valence bend angle. A transition state structure is labeled by the number 2, and local minima are denoted by numbers 3 and 4. (b) The spatial positions of the acetylene coordinates color-coded to match their corresponding location on the one-dimensional potential. The rightmost hydrogen retraces its path near the transition state but moves in concert with the leftmost hydrogen in the red-colored post transition state 2 regions.

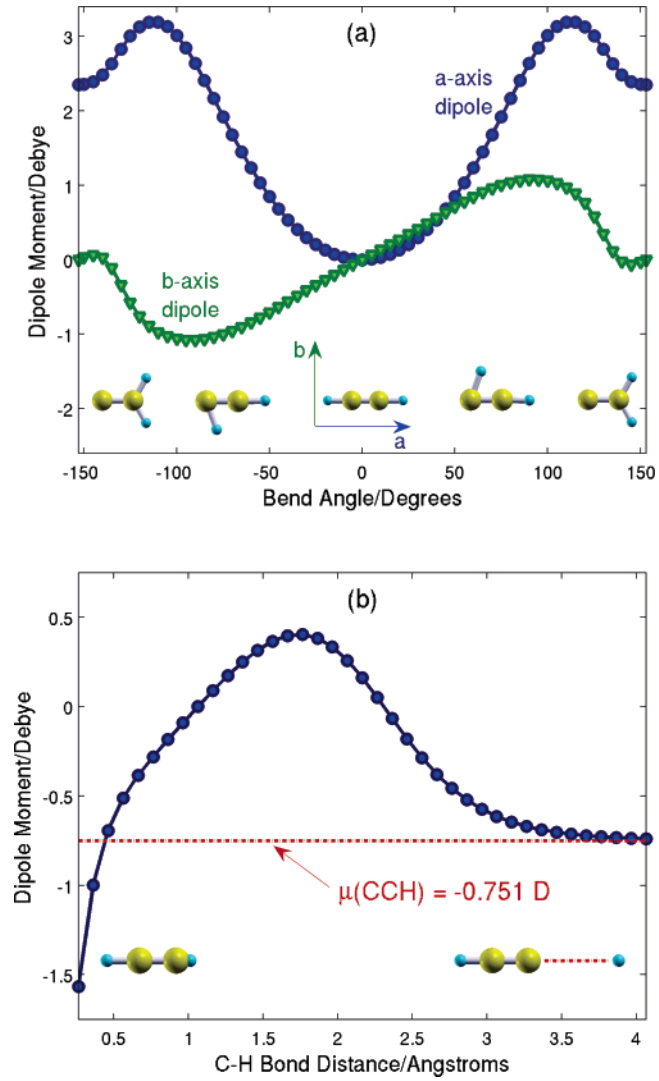

Figure 2. Dipole moments computed for relaxed geometries as a function of (a) fixed HCC local bend angle and (b) fixed local C−H stretch distance. In Figure 2a, the schematic diagrams of the bending motion show that when the local bend is excited, the *b*-axis dipole moment must change sign at $\theta = 0$. Conversely, the *a*-axis dipole moment is symmetric about $\theta = 0$ since the active hydrogen is always placed on identical horizontal distances along the *a*-axis during the (symmetric) local bending motion. In Figure 2b, the broken line indicates the numerical value of the dipole moment for the CCH equilibrium geometry. The dipole moments for Figures a and b were obtained from the CCSD(T)/cc-pVQZ and MR-AQCC/aug-cc-pVQZ levels of theory, respectively.

complete orthogonal set of basis functions is the set of complex exponentials

$$\left\{\frac{1}{\sqrt{2\pi}}, \frac{1}{\sqrt{2\pi}} e^{-ims}, \frac{1}{\sqrt{2\pi}} e^{ims}, m = 1,2,3,...\right\} \qquad (9)$$

Analytical expressions for the kinetic energy, potential energy, and dipole moment matrix elements are easily obtained from their Fourier series expansion coefficients.

For the local C−H stretch of acetylene, we chose the parameter *s* to be the single bond distance between the carbon and hydrogen atoms undergoing the large amplitude motion. Unlike the acetylene−vinylidene isomerization, the local stretch is not sufficiently well described by a CCSD(T) single-reference electronic configuration especially for large C−H bond distances. The electronic ground state of S_0 acetylene in its equilibrium geometry is qualitatively well described by CCSD(T) in which the carbon−hydrogen σ bond is doubly occupied. However, as the C−H bond is broken, the σ and σ^* orbitals become nearly degenerate, and the entire molecule (HCC$^\bullet$ + H$^\bullet$) becomes a diradical. An accurate description of the potential and dipole moments over this wide range of nuclear geometries requires the use of a multireference electronic wave function. Before proceeding with a detailed discussion of our ab initio methods for the local C−H stretch, we should mention that Lee and Taylor[36] have proposed the "T1 diagnostic" to determine whether a single-reference-based electron correlation procedure is appropriate. Based on their criterion, if the Euclidean norm of the t1 vector from a CCSD calculation is greater than 0.02, a multireference electron correlation method is necessary. We have computed the T1 diagnostic for the local C−H stretch and have found that T1 = 0.023 at a C−H bond distance of 2.256 Å using a cc-pVQZ basis. On the other hand, the T1 diagnostic for the acetylene−vinylidene transition state is 0.019 using an aug-cc-pVTZ basis, indicating that the isomerization is still qualitatively described by a single-reference configuration.

All multireference-based electronic structure calculations for the local C−H stretch were carried out with the Molpro 2002.6 package.[37] To minimize the errors caused by basis set truncation, we used the larger aug-cc-pVQZ basis set compared to the one used for the acetylene−vinylidene isomerization. The complete multireference calculation for each relaxed geometry was comprised of three separate steps. First, the ground-state molecular orbitals were calculated using the restricted Hartree−Fock (RHF) method. Next, to accurately describe the local stretch, we must include configurations occupying the σ^* C−H bond orbital; therefore, we used the multiconfiguration self-consistent field (MCSCF) method with the previous RHF orbitals as initial guesses for orbital optimization. In the MCSCF and subsequent electronic structure calculations, the 10 outermost molecular orbitals were selected as the active space which includes six σ and four π orbital symmetries. The outermost 10 electrons were placed in the active space, while the four electrons in the two lowest σ orbitals were kept doubly occupied but still optimized in all configurations. Last, to include electron correlation effects not accounted for in MCSCF methods, the final electronic wave function was constructed as single and double electronic excitations from MCSCF orbitals using the multireference averaged quadratic coupled cluster (MR-AQCC)[38] method. The MR-AQCC method is essentially a modified multireference procedure which approximately corrects for the size-consistency problem associated with the truncation of electronic excitations. We evaluated the relaxed MR-AQCC geometries and energies for C−H bond distances ranging from 0.26 to 4.06 Å in intervals of 0.1 Å. The dipole moment as a function of the local C−H stretch is shown in Figure 2b. The dotted horizontal line in this figure is the numerical value of the dipole moment for the HCC fragment evaluated at the relaxed MR-AQCC/aug-cc-pVQZ geometry. Each resulting geometry was translated to the center of mass frame, and all energies, dipole moments, and geometries were smoothly fit as a function of *s*. All of the matrix elements involving the C−H stretch of acetylene were evaluated using numerical quadrature.

IV. Dipole Moments in the Unsymmetrized Local Mode Basis

As previously noted, the inversion symmetry of acetylene prohibits both the existence of a permanent vibrational dipole moment and the corresponding typical pure-vibrational quadratic Stark effect. Our one-dimensional calculations are carried out in a space where *g/u* symmetry is not conserved. The resulting eigenfunctions are, therefore, not eigenfunctions of the inversion operator and may possess permanent vibrational dipole moments. To make the comparison with the experiment, we consider the local mode interpretation of the electric field induced perturbation investigated by Barnes et al. and demonstrate how the local mode limit of vibrational character leads to an effective dipole moment of the *g/u* components.

The matrix element that connects the optically bright and dark field-free eigenstates is an off-diagonal (in vibration) element of the electric dipole operator or a *dipole transition moment*, e.g., for a total of four quanta of C−H stretch, $\langle 04+|\mu|04-\rangle$. The local mode notation can be expressed in terms of the left and right oscillators,

$$|04\pm\rangle = \frac{1}{\sqrt{2}}[|04\rangle \pm |40\rangle] \tag{10}$$

where the notation on the right-hand side of eq 10 indicates $|v_{\text{left}}v_{\text{right}}\rangle$. The dipole matrix element can be re-expressed in the unsymmetrized basis as follows:

$$\langle 04+|\mu|04-\rangle = \frac{1}{2}[\langle 04|\mu|04\rangle - \langle 40|\mu|40\rangle] \tag{11}$$

Since, by symmetry, the two diagonal elements of the dipole operator in the unsymmetrized basis are of the same magnitude but of opposite sign,

$$\langle 04|\mu|04\rangle = -\langle 40|\mu|40\rangle \tag{12}$$

the perturbation matrix element in the symmetrized basis can be expressed as a diagonal matrix element in the left/right basis:

$$\langle 04+|\mu|04-\rangle = \langle 04|\mu|04\rangle \tag{13}$$

The transition dipole moment between the vibrational levels that make up the local mode pair can, therefore, be interpreted as a permanent vibrational dipole moment of an unsymmetrized state excited only in the right (or left) oscillator. Because the ± (*g/u*) components have been brought into near degeneracy, each rovibrational level now interacts with the rotational levels differing in *J* by one, of the *other* members of the local mode pair, through the dipole operator. The inversion symmetry has, therefore, been effectively broken because the physical consequences of the near degeneracy in the local mode limit are essentially identical to breaking the symmetry of the molecule through other means, e.g., isotopic substitution. That is, when the molecule is excited to a vibrational level that is in the local mode limit, it will exhibit regular quadratic Stark shifts, and it will be possible to excite "pure rotational" transitions in the millimeter-wave region.

An equivalent result holds in the case of the acetylene bending vibrations.

V. Local-Bending in the Polyad Model

The polyad model is a multiresonant effective Hamiltonian fitted to an extensive set of spectroscopic data.[7,39−42] Although the local-bending levels are not directly observed by any of the spectroscopic techniques and, therefore, not included in the fit, they emerge naturally from the effective Hamiltonian model. The local mode basis for bending levels is more complicated than that for the stretching levels because each CCH oscillator is treated as an isotropic two-dimensional harmonic oscillator and, therefore, is characterized by a vibrational angular momentum. In the symmetrized local mode basis, a state is labeled $|v_A^{\ell_A}, v_B^{\ell_B}\rangle_{\mathscr{L}}^{g/u\pm}$, where the $\ell_{A/B}$ refers to the vibrational angular momenta associated with the left or right local-bending mode (the total vibrational angular momentum is $\ell_{\text{tot}} = \ell_A + \ell_B$). While the extreme local-bender levels are denoted $|N_{\text{bend}}^0, 0^0\rangle_{\mathscr{L}}^{g/u\pm}$, the higher-lying levels are formed by removing one quantum of vibration from the highly excited oscillator and placing it in the less excited oscillator, e.g., $|(N_{\text{bend}}-1)^1, 1^{-1}\rangle_{\mathscr{L}}^{g/u\pm}$, $|(N_{\text{bend}}-2)^0, 2^0\rangle_{\mathscr{L}}^{g/u\pm}$, etc.

VI. Results

The agreement between the frequencies calculated from the one-dimensional ab initio model and the experimentally determined effective Hamiltonian model is generally good (<20 cm^{-1}) in the region where the local bender is believed to be an accurate description of the lowest members of each polyad (Figure 3). For the purpose of comparison with our one-dimensional calculations, the frequency of the local bending vibration is determined from the polyad model by calculating the energy difference between the lowest members of successive *gerade* pure-bending polyads with even values of N_{bend}, 0_g^+ and dividing by two. Between 18 and 19 quanta, the frequencies

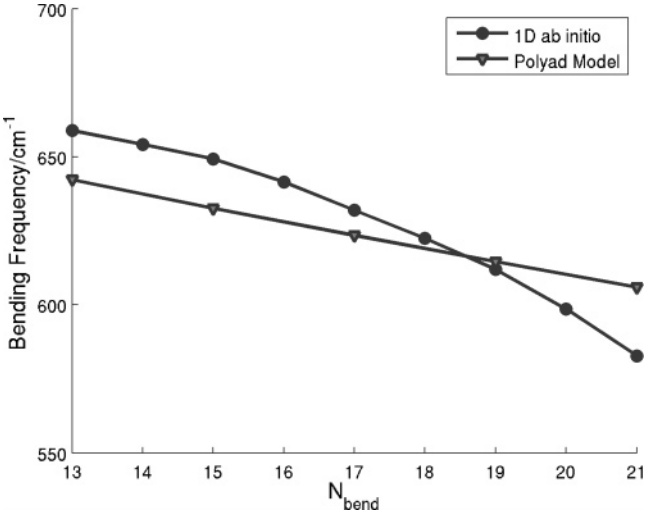

Figure 3. Experimentally derived polyad frequencies for a local CCH bending motion compared with one-dimensional ab initio calculations. The frequencies obtained from the polyad model and the ab initio calculations intersect between 18 and 19 quanta of N_{bend}.

calculated from the polyad model and those calculated from our one-dimensional cut through an ab initio potential pass through each other. The closely matched vibrational frequencies support the assertion that both models describe the same class of essentially one-dimensional large amplitude motion. This agreement is remarkable in light of the fact that the two calculations arise from drastic reductions in dimension of two very different (empirical vs ab initio) Hamiltonians.

As anticipated from our knowledge of the evolution of the vibrational character, the remarkable agreement occurs over a limited range. Below $N_{\text{bend}} = 10$, the disagreement between the two models reaches 50 cm^{-1} as the lowest members of the pure-bending polyads are well-described in the normal mode basis. Above 22 quanta of local bending, the ab initio frequency decreases rapidly, to values below 600 cm^{-1}, as the bending vibration starts to sample the barrier to isomerization (by tunneling through this barrier), and the approximately stationary hydrogen abruptly starts to migrate off axis to its vinylidene position. This behavior is not captured by the polyad model (because there is nothing barrier-related in the spectroscopic $\mathbf{H}^{\text{eff}}$), in which the vibrational frequency continues to decrease at a relatively constant rate.

VII. Evolution of the Dipole Moment

The ab initio vibrationally averaged dipole moments associated with the local stretching mode increase approximately linearly and start to decrease near the 11th vibrational state (Figure 4a). This trend can be associated with the increasing polarization of the C−H bond as internuclear distance increases. However, as the C−H bond is stretched, the polarization must reach a maximum (cf. Figure 2b), and at large internuclear distances the C−H bond must begin to break, leading to more neutral electron distributions for the H atom and HCC fragment ($\mu = -0.751$ D at the MR-AQCC/aug-cc-pVQZ level of theory). Since our one-dimensional calculations do not preserve g/u symmetry and are not eigenfunctions of the inversion operator, the vibrationally averaged dipole moment corresponding to the zero-point vibration is nonzero. As discussed in Section I, the definite g/u symmetry of every rovibrational level requires that the dipole moment of any eigenstate must be zero. To make meaningful comparisons to experimental data and other models, we have reported the vibrationally averaged dipole moments

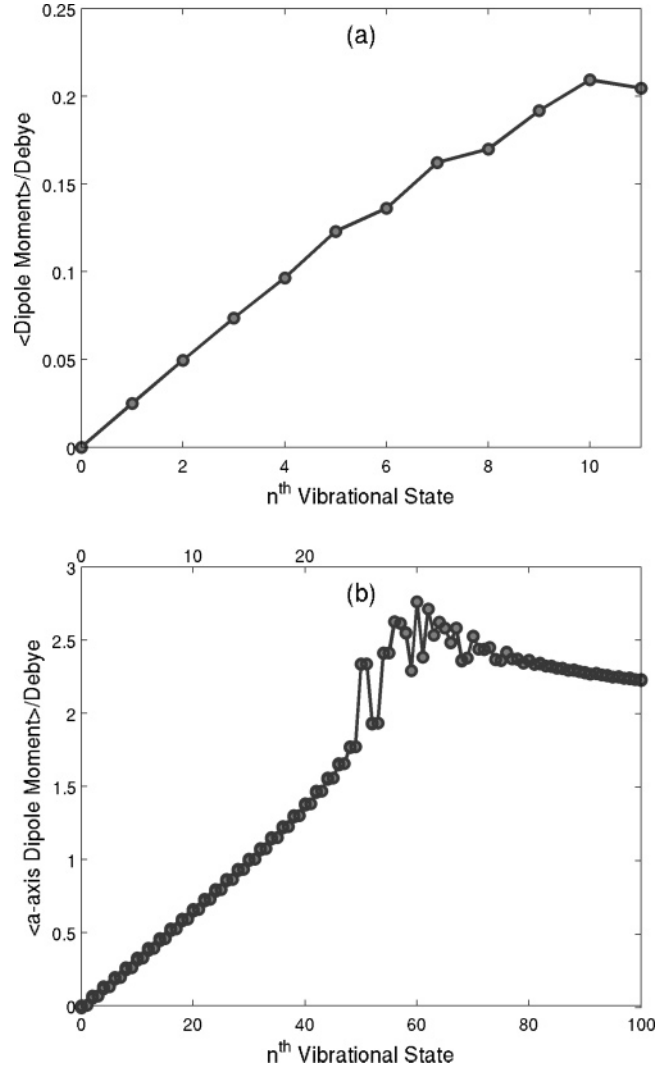

Figure 4. Vibrationally averaged ab initio dipole moments computed (a) for a local C−H stretch and (b) for a local bend. Since the *b*-axis dipole moment for the local bend is antisymmetric with respect to the equilibrium bend angle, its vibrational average is exactly zero, and only the vibrational average for the *a*-axis dipole is displayed. The bottom axis of Figure 4b is numbered according to the vibrational level in the fully permutational-symmetric isomerization path, and the top axis labels only the symmetric vibrational levels. Both averaged dipole moments are reported relative to the lowest vibrational quantum state.

relative to the lowest vibrational quantum state; i.e., the average dipole moments are bounded from below by zero. Our calculations may be compared with the experimental value from Barnes et al.[14] of 0.0696(12) for the dipole matrix element between the $|04+\rangle$ and $|04-\rangle$ local mode stretching states. Our calculated value of 0.0966 D is quite reasonable for our one-dimensional model. Some of this discrepancy is due to the fact that the acetylene stretching system, at this level of excitation, is in the *intermediate* case between the pure normal and pure local mode limits.[8] Experimental evidence that the local mode limit has not been reached is provided by the nonzero difference in vibrational excitation energies between the $|04+\rangle$ and $|04-\rangle$ states. The difference in energies has been measured to be 4.133(16) cm^{-1}. Our one-dimensional model will only apply to the pure local mode limit, while excitation of the other C−H bond oscillator must lead to a partial cancellation of the dipole due to its large amplitude motion. The experimental value embodies this partial cancellation, while our one-dimensional model does not.

TABLE 1: Energy Splittings between Lowest Members of the $g+$ and $u+$ Polyads and Calculated Dipole Moments for $N_{\mathrm{Bend}} = 14-26$.[a]

N_{bend}	$E(\lvert N^0_{\mathrm{bend}},0^0\rangle^{g+}_{\ell})$	$E(g+)$-$E(u+)$	μ (D)	$E(\lvert(N_{\mathrm{bend}}-1)^1,1^{-1}\rangle^{g+}_{\ell})$	$E(g+)$-$E(u+)$	μ (D)	$E(\lvert(N_{\mathrm{bend}}-2)^0,2^0\rangle^{g+}_{\ell})$	$E(g+)$-$E(u+)$	μ (D)
14	8972.1	-1×10^{-4}	0.85	9070.0*	-9		9037.0*	-4×10^{-2}	
16	10236.9	-3×10^{-5}	1.02	10352.4*	-4×10^{-2}		10315.6	3×10^{-3}	0.78
18	11485.0	-4×10^{-6}	1.20	11605.7	6×10^{-5}	1.01	11574.7	2×10^{-4}	0.93
20	12717.4	-4×10^{-7}	1.36	12844.8	7×10^{-5}	1.18	12815.7	-8×10^{-6}	1.07
22	13934.9	-4×10^{-8}	1.55	14070.2	8×10^{-6}	1.36	14040.2	-2×10^{-6}	1.20
24	15137.9	-1×10^{-9}	1.77	15289.9	3×10^{-7}	1.54	15249.3	-1×10^{-7}	1.39
26	16327.1	3×10^{-10}	2.28	16480.1	-8×10^{-8}	1.76	16443.9	1×10^{-8}	1.54

[a] All energies and energy differences reported are in units of cm^{-1}. Energies denoted by an asterisk are not well-described in the local mode basis using the Hose−Taylor criterion. The increase in dipole moment is accompanied by decreasing energy differences between corresponding low-energy edge members of the $g+$ and $u+$ polyads.

The one-dimensional model can be corrected for the admixture of other local mode basis states if the eigenvectors of the polyad can be obtained from diagonalization of an effective Hamiltonian constructed in the local mode basis. Using the local mode parameters of Halonen,[5] the nominal $|40-\rangle$ state is 92.7% $|40-\rangle$ and 7.3% $|31-\rangle$. Estimates for the dipole moments of the nonextreme states are obtained by subtracting the number of quanta of excitation in the two oscillators, $n_A - n_B$, and assigning the value of the dipole moment from the one-dimensional treatment where the level of excitation is taken to be $n_A - n_B$, i.e., $\mu(|31\rangle) = \mu(|20\rangle)$. This results in only a small correction to our calculated value, from 0.0966 to 0.0926 D.

Figure 4b shows the vibrationally averaged dipole moments for the full permutationally symmetric isomerization path with respect to the interchange of the two H atoms. The bottom axis of Figure 4b is numbered according to the vibrational level in this symmetric $H_aC_bC_cH_d \rightleftharpoons H_dC_bC_cH_a$ double-well potential. Because of this symmetry, the lowest average dipole moments come in pairs corresponding to nuclear permutational splittings between symmetric and antisymmetric vibrational states. Throughout this work we use the numbering scheme shown on the top axis of Figure 4b, which only labels the symmetric vibrational states in our one-dimensional bending model. It can be seen that the vibrationally averaged dipole moments obey a nearly linear trend up to 22 quanta of vibrational excitation, increasing approximately 0.068 D per quantum of excitation. As in the case of the C−H stretching, our calculated value overestimates the value available from experiment. The value of the slope obtained from the relatively low energy excited states of acetylene-*d* by Matsumura et al.,[17] 0.046 D, is, in a manner similar to that of the C−H stretching modes, not reflective of the pure CCH bending motion. Examination of the normal mode eigenvectors, obtained from an **FG** matrix analysis based on the force constants of Strey and Mills,[43] reveals that significant CCD bending motion occurs in the nominally CCH bending mode, ν_5. The calculated dipole moment variation, in the linear region, is qualitatively due to the diminishing projection of the C−H bond dipole on the C−C bond axis, leading to an imbalance of the bond dipoles of the two C−H fragments. In the same energy region where the vibrational frequency begins to decrease rapidly, the dipole moment increases more rapidly due to increased sampling of the isomerization barrier (3.0 D) and mixing with the vinylidene configuration (2.5 D).

The $v = 25$ excited vibrational level identified in the calculation clearly deviates from the smooth linear trend of the lower-lying states. This level is associated with the zero-point level of S_0 vinylidene. Near the $v = 25$ vibrational level, the averaged dipole moments begin to change discontinuously since the vibrational wave function begins to sample both the acetylene and vinylidene minima. Above this energy, the dipole moment oscillates between acetylene-localized states and values more typical of the isomerization transition state before approaching a constant value of 2.1 D at high local-bend excitation.

VIII. Assignment of Large Amplitude Local Bender States

Although we have primarily focused on the extreme local bender levels, those that lie at the bottom of each pure-bending polyad, it is important to note that the other members of pure-bending polyads can be described in the local mode basis. Examination of the eigenfunctions obtained from the polyad model reveals a transition from normal to local-bend character at approximately 14 quanta of bending vibration, at which point the lowest member of each pure-bending polyad is best described by a local CCH bending motion.[7] This qualitative change in vibrational character is accompanied by a decreasing energy difference between the lowest members of the 0^+_g and 0^+_u polyads. At $N_{\mathrm{bend}} = 10$, this energy difference is > 10 cm^{-1}, but it rapidly decreases to $< 10^{-3}$ cm^{-1} by $N_{\mathrm{bend}} = 14$, and $< 10^{-7}$ cm^{-1} by $N_{\mathrm{bend}} = 22$. In Table 1 we compare the energy splittings between the lowest members of the $g+$ and $u+$ polyads for $N_{\mathrm{bend}} = 14-26$. These lowest *extreme local bender* levels form a local mode pair, and the transition dipole that couples them can be viewed as a permanent vibrational dipole moment, as in the case of the acetylene C−H stretching levels discussed in Section VII.

Due to the systematic near degeneracies between extreme local bender levels of opposite vibrational parities, the eigenstates at the low energy edge of the local-bender polyads are poised for symmetry breaking. The mechanism of this symmetry breaking depends on the value of the vibrational angular momentum. Levels with no vibrational angular momentum ($\ell_{\mathrm{tot}} = 0$) have a single vibrational parity; the total parity and nuclear spin symmetry alternate with J. In the local mode limit, each rovibrational level from a 0^+_g polyad becomes degenerate with one from the corresponding 0^+_u polyad. However, these degenerate levels are of the same parity (and different nuclear spin symmetry) and, therefore, cannot interact via the Stark effect. Rather, there is a nonzero $\Delta J = 1$ matrix element between adjacent rotational levels of the two polyads (e.g., 0^+_g $J = 0$, 0^+_u $J = 1$) which have the correct parities and nuclear spin symmetries to interact via the electric dipole operator. The $\Delta J = 1$ matrix element leads to a quadratic Stark effect analogous to that observed in nonsymmetric linear molecules or symmetric top molecules with $K = 0$. Vibrational levels with nonzero angular momentum ($\ell_{\mathrm{tot}} > 0$) have both vibrational parities. An isolated $\ell_{\mathrm{tot}} > 0$ vibrational state has, for each value of J, a pair of levels with opposite parities. In acetylene, and symmetric molecules in general, these levels cannot interact due to their differing nuclear spin symmetries. As for the $\ell_{\mathrm{tot}} = 0$ case, in the local mode limit, a rovibrational level of a given

polyad becomes degenerate with a corresponding level in a polyad of the opposite symmetry (e.g., $\Delta_g \leftrightarrow \Delta_u$). The levels which have become degenerate satisfy the condition that nuclear spin symmetry must be conserved for interaction via the Stark operator. The $\Delta J = 0$ interaction between the degenerate levels will lead to a linear Stark effect, analogous to those observed in symmetric top molecules with $K > 0$.

The ability to equate the one-dimensional calculation of the dipole moment with the dipole created by imbalance in excitation of oscillators has significant predictive power. It enables us to assign dipole moments to any basis state in the local mode limit and therefore allows the calculation of the dipole moment for each eigenstate based on the eigenvectors in the local mode basis. Predictions of the dipole moments for the three lowest energy eigenstates of the $N_{\text{bend}} = 14-26$ polyads are found in Table 1. Predictions are made in the same manner as for the stretching case by neglecting the vibrational angular momentum, i.e., $\mu(|14^2,2^{-2}\rangle_{\mathscr{L}}) = \mu(|14^0,2^0\rangle_{\mathscr{L}})$. These lowest eigenstates are assigned to the local mode states as $|N^0_{\text{bend}},0^0\rangle^{g+}_{\mathscr{L}}$, $|(N_{\text{bend}} - 1)^1,1^{-1}\rangle^{g+}_{\mathscr{L}}$, and $|(N_{\text{bend}} - 2)^0,2^0\rangle^{g+}_{\mathscr{L}}$ respectively, although only the lowest energy state in the $N_{\text{bend}} = 14$ polyad can be assigned based on the Hose−Taylor criterion.[44] As we move toward the center of each polyad, the local mode model describes each eigenstate less well. That is, the eigenstates contain larger contributions from several local mode basis states, including those with smaller differences in excitation between the two oscillators. This trend causes the dipole moment to decrease faster than linearly inside a given polyad, although at high excitation ($N_{\text{bend}} \sim 22$) all of the listed states are described well by the local mode basis.

The shape of the *a*-axis dipole moment function strongly resembles that of the potential energy surface. The maximum value of the *a*-axis dipole is reached near the transition state of the isomerization reaction, before the approximately stationary hydrogen begins to move off axis to form vinylidene. This near transition state configuration represents the largest distortion of the electronic wave function. This is ideal for our goal to perform high-resolution "transition state spectroscopy" because the larger dipole moments are more readily observable via laser Stark spectroscopy.

Even more useful is the ability to identify particular vibrational levels based on our predictions of variation in electronic structure. While we have described electronic signatures of only two one-dimensional motions, vibrational states that do not consist of these special motions are expected to be highly dynamically mixed. The ergodic nature of the highly mixed vibrational levels imply that they will remain essentially silent to Stark effect measurements, except in the case of accidental near degeneracies. The large amplitude states will be the only states with significant, regular Stark activity.

IX. Conclusions

We have explored a one-dimensional reduction of the full seven-dimensional ab initio potential energy surface of the C_2H_2 S_0 electronic state and found that it strongly resembles the one-dimensional, local bending reduction of the empirical spectroscopic pure-bend effective Hamiltonian. These reductions in dimension occur when the large amplitude motion decouples from the other nuclear motions as a result of anharmonic detuning from resonance. A comparison between the computed frequencies of the one-dimensional ab initio potential and those of the spectroscopic effective Hamiltonian, the parameters of which are refined against experimental data, exhibits good agreement for the local bending motion. The results of Section VI strongly indicate reduction of both ab initio and spectroscopic Hamiltonians to the same one-dimensional potential even though the two Hamiltonians are derived via completely different reductive formalisms. This is particularly noteworthy since the spectroscopic effective Hamiltonian does not explicitly specify the displacement coordinates of the stable, one-dimensional, localized, motion, but this one-dimensional path is explicitly defined in our reaction path Hamiltonian. More importantly, the large-amplitude local vibrations which lead to changes in the electronic properties of acetylene, result in a nonzero transition dipole between the two nearly degenerate *g*/*u* eigenstates associated with the local mode. This near-degeneracy of the local mode pair, which indicates the *g*/*u* symmetry is ready to be broken, is a hallmark of local mode behavior. We propose the large changes in dipole moments along the local bending coordinate provide a method to identify particular vibrational levels via the Stark effect. The dipole moment values computed from the ab initio one-dimensional potential will be useful in distinguishing extreme local mode states from the vastly more numerous strongly mixed isoenergetic states. In addition, the dipole moments will help assign members of the $|N_{\text{bend}},0\rangle^{g/u\pm}_{\mathscr{L}}$, $|N_{\text{bend}} - 1,1\rangle^{g/u\pm}_{\mathscr{L}}$, $|N_{\text{bend}} - 2,2\rangle^{g/u\pm}_{\mathscr{L}}$, etc. family of states. This information is essential because once the energies of such assigned states are obtained from spectra, the one-dimensional local mode potential can be experimentally refined. The relative energies of the $\{|N_{\text{bend}},0\rangle^{g/u\pm}_{\mathscr{L}},|N_{\text{bend}} - 1,1\rangle^{g/u\pm}_{\mathscr{L}},|N_{\text{bend}} - 2,2\rangle^{g/u\pm}_{\mathscr{L}}\}$ and $\{|N_{\text{bend}} + 1,0\rangle^{u/g\pm}_{\mathscr{L}},|N_{\text{bend}},1\rangle^{u/g\pm}_{\mathscr{L}},|N_{\text{bend}} - 1,2\rangle^{u/g\pm}_{\mathscr{L}}\}$, etc. groups of local mode states, supplemented by measured dipole moments, provide direct experimental characterization of the reaction coordinate proximal to the barrier maximum.

Acknowledgment. A. H. S. acknowledges support from the Army Research Office under a National Defense Science and Engineering Graduate Fellowship. This research was supported by the Office of Basic Energy Sciences, Offices of Energy Research, U.S. Department of Energy under grant no. DE-FG0287ER13671.

References and Notes

(1) Reese, J. A.; Nguyen, T. V.; Korter, T. M.; Pratt, D. W. *J. Am. Chem. Soc.* **2004**, *126*, 11387−11392.
(2) Bowman, J. M.; Irle, S.; Morokuma, K.; Wodtke, A. *J. Chem. Phys.* **2001**, *114*, 7923−7934.
(3) Jung, C.; Taylor, H. S.; Jacobson, M. P. *J. Phys. Chem. A* **2001**, *105*, 681−693.
(4) Halonen, L.; Child, M. S.; Carter, S. *Mol. Phys.* **1982**, *47*, 1097−1112.
(5) Halonen, L. *Adv. Chem. Phys.* **1998**, *104*, 41−179.
(6) Yang, S. F.; Halonen, L., Camparague, A. *Mol. Phys.* **2001**, *99*, 1303−1309.
(7) Jacobson, M. P.; Silbey, R. J.; Field, R. W. *J. Chem. Phys.* **1999**, *110*, 845−859.
(8) Scherer, G. J.; Lehmann, K. K.; Klemperer, W. *J. Chem. Phys.* **1983**, *78*, 2817−2832.
(9) Lehmann, K. K. *J. Chem. Phys.* **1992**, *96*, 8117−8119.
(10) Prosmiti, R.; Farantos, S. C. *J. Chem. Phys.* **1995**, *103*, 3299−3314.
(11) Prosmiti, R.; Farantos, S. C. *J. Chem. Phys.* **2003**, *118*, 8275−8280.
(12) Rose, J. P.; Kellman, M. E. *J. Chem. Phys.* **1996**, *105*, 10743−10754.
(13) Sibert, E. L.; McCoy, A. B. *J. Chem. Phys.* **1996**, *105*, 469−478.
(14) Barnes, J. A.; Gough, T. E.; Stoer, M. *Chem. Phys. Lett.* **1995**, *237*, 437−442.
(15) Barnes, J. A.; Gough, T. E.; Stoer, M. *J. Chem. Phys.* **2001**, *114*, 4490−4495.
(16) Muenter, J. S.; Laurie, V. W. *J. Am. Chem. Soc.* **1964**, *86*, 3901−3902.
(17) Matsumura, K.; Tanaka, T.; Endo, Y.; Saito, S.; Hirota, E. *J. Phys. Chem.* **1980**, *84*, 1793−1797.
(18) Rainer, S.; Köppel, H. *J. Chem. Phys.* **2001**, *115*, 7907−7923.
(19) Bittner, M.; Köppel, H. *Phys. Chem. Chem. Phys.* **2003**, *5*, 4604−4611.
(20) Zou, S.; Bowman, J. M. *Chem. Phys. Lett.* **2003**, *368*, 421−424.

(21) Zou, S.; Bowman, J. M.; Brown, A. *J. Chem. Phys.* **2003**, *118*, 10012−10023.
(22) Xu, D.; Li, G.; Xie, D.; Guo, H. *Chem. Phys. Lett.* **2002**, *365*, 480−486.
(23) Tew, D. P.; Handy, N. C.; Carter, S.; Irle, S.; Bowman, J. M. *Mol. Phys.* **2003**, *101*, 3513−3525.
(24) Hougen, J. T.; Bunker, P. R.; Johns, J. W. C. *J. Mol. Spectrosc.* **1970**, *34*, 136−172.
(25) Szalay, V. *J. Mol. Spectrosc.* **1988**, *128*, 24−61.
(26) Miller, W. H.; Handy, N. C.; Adams, J. E. *J. Chem. Phys.* **1980**, *72*, 99−112.
(27) Fukui, K. *J. Phys. Chem.* **1970**, *74*, 4161−4163.
(28) Fukui, K. *Acc. Chem. Res.* **1981**, *14*, 363−368.
(29) Wong, B. M.; Thom, R. L.; Field, R. W. *J. Phys. Chem. A.* **2006**, *110*, 7406−7413.
(30) Frisch, M. J.; Trucks, G. W.; Schlegel, H. B.; Scuseria, G. E.; Robb, M. A.; Cheeseman, J. R.; Montgomery, J. A., Jr.; Vreven, T.; Kudin, K. N.; Burant, J. C.; Millam, J. M.; Iyengar, S. S.; Tomasi, J.; Barone, V.; Mennucci, B.; Cossi, M.; Scalmani, G.; Rega, N.; Petersson, G. A.; Nakatsuji, H.; Hada, M.; Ehara, M.; Toyota, K.; Fukuda, R.; Hasegawa, J.; Ishida, M.; Nakajima, T.; Honda, Y.; Kitao, O.; Nakai, H.; Klene, M.; Li, X.; Knox, J. E.; Hratchian, H. P.; Cross, J. B.; Bakken, V.; Adamo, C.; Jaramillo, J.; Gomperts, R.; Stratmann, R. E.; Yazyev, O.; Austin, A. J.; Cammi, R.; Pomelli, C.; Ochterski, J. W.; Ayala, P. Y.; Morokuma, K.; Voth, G. A.; Salvador, P.; Dannenberg, J. J.; Zakrzewski, V. G.; Dapprich, S.; Daniels, A. D.; Strain, M. C.; Farkas, O.; Malick, D. K.; Rabuck, A. D.; Raghavachari, K.; Foresman, J. B.; Ortiz, J. V.; Cui, Q.; Baboul, A. G.; Clifford, S.; Cioslowski, J.; Stefanov, B. B.; Liu, G.; Liashenko, A.; Piskorz, P.; Komaromi, I.; Martin, R. L.; Fox, D. J.; Keith, T.; Al-Laham, M. A.; Peng, C. Y.; Nanayakkara, A.; Challacombe, M.; Gill, P. M. W.; Johnson, B.; Chen, W.; Wong, M. W.; Gonzalez, C.; Pople, J. A. *Gaussian 03*, revision C.02; Gaussian, Inc.: Wallingford, CT, 2004.
(31) Kendall, R. A.; Dunning, T. H., Jr.; Harrison, R. J. *J. Chem. Phys.* **1992**, *96*, 6796−6806.
(32) Liu, L.; Muckerman, J. T. *J. Chem. Phys.* **1997**, *107*, 3402−3416.
(33) Xu, D.; Li, G.; Xie, D.; Guo, H. *Chem. Phys. Lett.* **2002**, *365*, 480−486.
(34) Xu, D.; Chen, R.; Guo, H. *J. Chem. Phys.* **2003**, *118*, 7273−7282.
(35) Bačić, Z.; Light, J. C. *J. Chem. Phys.* **1986**, *85*, 4594−4604.
(36) Lee, T. J.; Taylor, P. R. *Int. J. Quantum Chem.* **1989**, *S23*, 199−207.
(37) MOLPRO, a package of ab initio programs designed by Werner, H.-J.; Knowles P. J., version 2002.6, Amos, R. D.; Bernhardsson, A.; Berning, A.; Celani, P.; Cooper, D. L.; Deegan, M. J. O.; Dobbyn, A. J.; Eckert, F.; Hampel, C.; Hetzer, G.; Knowles, P. J.; Korona, T.; Lindh, R.; Lloyd, A. W.; McNicholas, S. J.; Manby, F. R.; Meyer, W.; Mura, M. E.; Nicklass, A.; Palmieri, P.; Pitzer, R.; Rauhut, G.; Schütz, M.; Schumann, U.; Stoll, H.; Stone, A. J.; Tarroni, R.; Thorsteinsson, T.; and Werner, H.-J.
(38) Szalay, P. G.; Bartlett, R. J. *Chem. Phys. Lett.* **1993**, *214*, 481−488.
(39) El Idrissi, M. I.; Lievin, J.; Camparague, A.; Herman, M. *J. Chem. Phys.* **1999**, *110*, 2074−2086.
(40) Hoshina, K.; Iwasaki, A.; Yamanouchi, K.; Jacobson, M. P.; Field, R. W. *J. Chem. Phys.* **2001**, *114*, 7424−7442.
(41) Temsamani, M. A.; Herman, M. *J. Chem. Phys.* **1995**, *102*, 6371−6384.
(42) Temsamani, M. A.; Herman, M.; Solina, S. A. B.; O'Brien, J. P.; Field, R. W. *J. Chem. Phys.* **1996**, *105*, 11357−11359.
(43) Strey, G.; Mills, I. M. *J. Mol. Spectrosc.* **1976**, *59*, 103−115.
(44) Hose, G.; Taylor, H. S. *J. Chem. Phys.* **1982**, *76*, 5356−5364.